ChemComm

Dual functional catalysis of $[Nb_6O_{19}]^{8-}$-modified Au/Al_2O_3

Journal:	*ChemComm*
Manuscript ID	CC-COM-05-2022-002472.R2
Article Type:	Communication

COMMUNICATION

Dual functional catalysis of $[Nb_6O_{19}]^{8-}$-modified Au/Al_2O_3

Soichi Kikkawa,[a,b] Shoji Fukuda,[a] Jun Hirayama,[a,b] Naoki Shirai,[a] Ryo Takahata[c], Kosuke Suzuki,[d,e] Kazuya Yamaguchi,[d] Toshiharu Teranishi,[c] and Seiji Yamazoe*[a,b,e]

Received 00th January 20xx,
Accepted 00th January 20xx

DOI: 10.1039/x0xx00000x

A catalyst prepared by modifying the surface of Au nanoparticles (NPs) on Al_2O_3 with $[Nb_6O_{19}]^{8-}$ clusters had specific base and reduction abilities, and the reduction of *p*-nitrophenol to *p*-aminophenol using H_2 as a reductant proceeded efficiently with the dual functional catalyst. At the interface between Au NPs and basic $[Nb_6O_{19}]^{8-}$, heterolytically cleaved hydrogen species are generated, which can efficiently react with a nitrophenolate ion generated by base catalysis. Moreover, this surface modification strategy was applicable to the reduction of other nitro compounds.

Catalytic reduction using H_2 as a reductant is one of the most promising techniques for synthesizing the desired chemical compounds, and supported metal NP catalysts have been developed up to now from the viewpoint of their low cost and reusability.[1-6] The catalytic-reduction activity and selectivity of supported metal NPs can be controlled by the size, composition, shape, and electronic states of the metal NPs, as well as the choice of supports, since the activation of H_2 and substrates take place on the metal NPs surface or at the interface between the metal NPs and the support. Therefore, the design of the surface and interface of supported metal NP catalysts is crucially important for the development of efficient reduction catalysts using H_2.

Surface modification of metal NPs by organic ligands and/or metal oxides has attracted much attention for developing highly active and chemoselective catalysts.[7-9] For example, selective oxidation of benzyl alcohol to benzaldehyde can be achieved by surface modification of supported Au clusters using thiolate ligands, which suppresses the overoxidation to benzoic acid by electron withdrawal from Au cluster and the undesired esterification by steric hindrance.[9] Mitsudome *et al*. reported that an Ag NP core–CeO_2 shell nanocomposite catalyst exhibits chemoselective reduction catalysis for various nitro compounds and epoxides by heterolytic cleavage of H_2 at the interface between Ag NP and base site of CeO_2.[7] Similar chemoselective reduction of nitro compounds have been achieved over ligand-stabilized Ir NPs; a partially oxidized area on the Ir NPs selectively adsorbs polar nitro group which is reduced by the activated hydrogen species on the Ir NP surface.[8] However, surface modification methods of supported metal NPs are limited, and the development of more versatile methods is a challenging issue.

Metal oxide clusters, called as polyoxometalates (POMs), that are composed of dozens of metal atoms show unique characters far from their bulk metal oxides and have been applied to acid catalysts[10, 11] and photocatalysts.[12, 13] Since the discovery of basic POMs such as $[HGeW_{10}O_{36}]^{7-}$,[14] $[H_4SiW_{11}O_{39}]^{4-}$,[15] and $[SiW_{10}O_{34}(H_2O)_2]^{4-}$,[16] the base catalytic application of POMs has been much attention. Our group has recently reported that group V metal oxide clusters, such as $[Ta_6O_{19}]^{8-}$, $[Nb_6O_{19}]^{8-}$, and $[Nb_{10}O_{28}]^{6-}$, exhibited efficient base catalysis for Knoevenagel condensation and CO_2 fixation reactions.[17-20] Especially, $[Ta_6O_{19}]^{8-}$ and $[Nb_6O_{19}]^{8-}$ exhibited strong Brønsted base catalysis to abstract protons from nitriles with a pK_a value of 23.8. From the DFT calculation that those clusters possess highly negatively-charged O sites, their highly negatively-charged O sites would be acted as the basic sites.[19]

The supported Au clusters and nanoparticles were active for reduction reactions of nitro groups using H_2 molecule.[2, 21] The surface modification of Au NPs by anionic metal oxide clusters is expected to develop dual-functional catalysts having both reduction and base catalytic properties. Herein, we newly designed a dual functional catalyst by modifying the surface of Al_2O_3-supported Au NPs with basic $[Nb_6O_{19}]^{8-}$ (Nb6-Au/Al_2O_3). Weinstock group has reported that anionic metal oxide clusters, such as $[AlW_{11}O_{39}]^{9-}$, $[SiW_{11}O_{39}]^{8-}$, $[PW_{11}O_{39}]^{7-}$, and $[Nb_6O_{19}]^{8-}$, can coordinate to the surface of Au NPs as protective ligands in a homogeneous system. The negatively charged oxygen atoms of metal oxide clusters afford the electronic donation to the Au NPs surface and the counter cations neutralized the total charge of the composites.[22-27] Nakagawa *et al*. reported that

[a] *Department of Chemistry, Graduate School of Science, Tokyo Metropolitan University, 1-1 Minami-osawa, Hachioji, Tokyo 192-0397, Japan.*
[b] *Elements Strategy Initiative for Catalysts & Batteries (ESICB), Kyoto University, 1-30 Goryo-Ohara, Nishikyo-ku, Kyoto 615-8245, Japan.*
[c] *Institute for Chemical Research, Kyoto University, Gokasho, Uji, Kyoto 611-0011, Japan.*
[d] *Department of Applied Chemistry, School of Engineering, The University of Tokyo, 7-3-1 Hongo, Bunkyo-ku, Tokyo 113-8656, Japan.*
[e] *Precursory Research for Embryonic Science and Technology (PRESTO), Japan Science and Technology Agency (JST), Tokyo 102-0076, Japan.*
† Footnotes relating to the title and/or authors should appear here.
Electronic Supplementary Information (ESI) available: [details of any supplementary information available should be included here]. See DOI: 10.1039/x0xx00000x

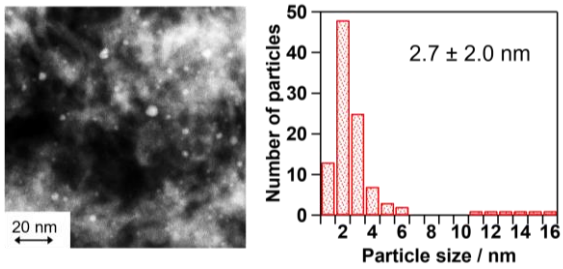

Fig.1 HAADF-STEM image and the size distribution of the observed NPs in Nb6-Au/Al_2O_3.

$[SiVW_{11}O_{40}]^{5-}$ was coordinated on the surface of supported Rh NPs during the reduction of Rh species in the presence of H_2.[28] In this study, we attempted to develop a simple synthesis method by just mixing $[Nb_6O_{19}]^{8-}$ with Au/Al_2O_3 in an aqueous solution and the following centrifugation; $[Nb_6O_{19}]^{8-}$ was easily adsorbed on the surface of Au NPs on Al_2O_3 without ligand-exchange process. In addition, Nb6-Au/Al_2O_3 exhibited dual functional catalysis having both base and reduction abilities, acting as an efficient heterogeneous catalyst for selective reduction of *p*-nitrophenol, nitrobenzene, and *p*-nitrostyrene without extra-base addition.

Nb6-Au/Al_2O_3 was prepared via a very simple method of adsorbing $[Nb_6O_{19}]^{8-}$ species on pre-prepared Au/Al_2O_3 (Au NP size: 2.0 ± 0.8 nm, Fig. S1) in an aqueous solution (see ESI†). From inductively coupled plasma Auger electron spectroscopy (ICP-AES) analysis of Nb6-Au/Al_2O_3, the loading amounts of Au NPs and $[Nb_6O_{19}]^{8-}$ as metal oxide clusters were determined to be respectively (Table S1). Fig. S2 shows the powder X-ray diffraction (XRD) patterns of the Nb6-Au/Al_2O_3, Au/Al_2O_3, and Al_2O_3. In the XRD patterns of Au/Al_2O_3 and Nb6-Au/Al_2O_3, no peaks attributed to bulk Au metal with a face-centered cubic structure were observed. It was also confirmed that crystalline $K_8Nb_6O_{19}{\cdot}nH_2O$ was not formed in Nb6-Au/Al_2O_3. This suggested that the modification of Au NPs did not significantly increase the size of the original Au NPs in Au/Al_2O_3 and that $[Nb_6O_{19}]^{8-}$ was dispersedly supported on the catalyst surface. Fig. 1 shows the high-angle annular dark-field scanning transmission electron microscope (HAADF-STEM) image and the particle size distribution in Nb6-Au/Al_2O_3. The average diameter of the observed nanoparticles was found to be 2.7 ± 2.0 nm, suggesting that only a small portion of Au aggregation occurred in this modification method, or due to the adsorption of

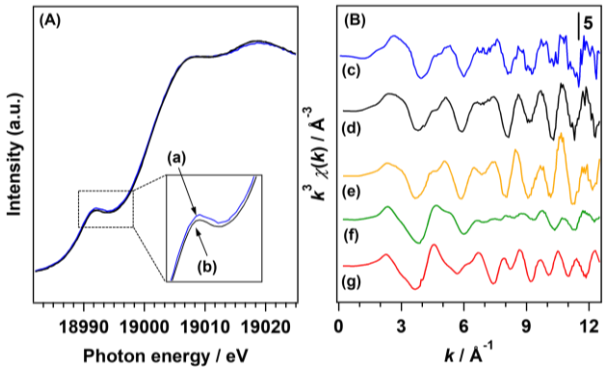

Fig. 2(A) Nb K-edge XANES spectra of (a) Nb6-Au/Al_2O_3 and (b) an aqueous solution of $K_8Nb_6O_{19}$. **(B)** Nb K-edge EXAFS oscillations of (c) Nb6-Au/Al_2O_3, (d) the $K_8Nb_6O_{19}$ solution, (e) $K_8Nb_6O_{19}{\cdot}14H_2O$, (f) $Nb_2O_5{\cdot}nH_2O$, and (g) Nb_2O_5.

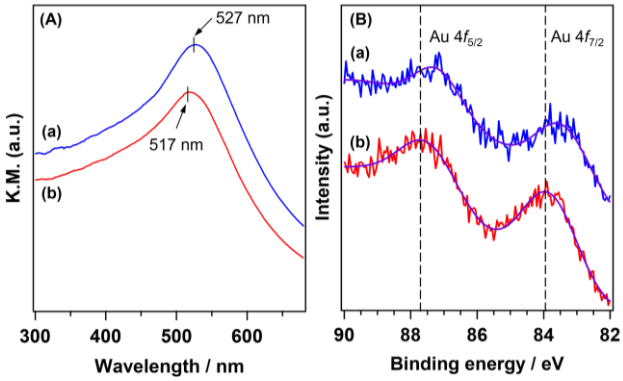

Fig.3(A) DR-UV-vis spectra and **(B)** XPS spectra of (a) Nb6-Au/Al_2O_3 and (b) Au/Al_2O_3.

$[Nb_6O_{19}]^{8-}$ on the Au NP surface. It was confirmed by the line analysis of Nb6-Au/Al_2O_3 using an energy dispersive X-ray (EDX) microanalyzer that $[Nb_6O_{19}]^{8-}$ was mainly located on the Au NPs (Fig. S3). From the above-mentioned characterization results, we concluded that $[Nb_6O_{19}]^{8-}$ was coordinated to the surface of Au NPs by the proposed very simple adsorption method.

The coordination of $[Nb_6O_{19}]^{8-}$ to the Au NPs surface was further supported by X-ray absorption spectroscopy (XAS) analysis (Fig. 2). The Nb K-edge X-ray absorption near-edge structure (XANES) spectrum of Nb6-Au/Al_2O_3 was similar to that of an aqueous solution of $K_8Nb_6O_{19}$; however, the pre-edge peak intensity of Nb6-Au/Al_2O_3 in the Nb K-edge XANES spectrum slightly increased in comparison with that of the $K_8Nb_6O_{19}$ solution. This increase indicates the distortion of the {NbO_6} octahedral structure in $[Nb_6O_{19}]^{8-}$ by its coordination to the Au/Al_2O_3.[29] On the other hand, the $[Nb_6O_{19}]^{8-}$ structure maintained even after the coordination to the Au NPs on Al_2O_3 because the Nb-K edge extended X-ray absorption fine structure (EXAFS) spectrum of Nb6-Au/Al_2O_3 (Fig. 2B and Fig. S4) was in accordance with those of solid $K_8Nb_6O_{19}{\cdot}14H_2O$ and $K_8Nb_6O_{19}$ solution, whose structures were confirmed by XRD and FT-IR (Fig. S5).

Fig. 3A shows the diffuse reflectance (DR)-UV-vis spectra of Nb6-Au/Al_2O_3 and Au/Al_2O_3. In the spectrum of Au/Al_2O_3, an absorption peak at 517 nm assignable to localized surface plasmon resonance (LSPR) of Au NPs on the supports was clearly observed. The LSPR peak was shifted to higher energy by the coordination of $[Nb_6O_{19}]^{8-}$. The anionic metal oxide clusters, such as $[SiW_{11}O_{39}]^{8-}$ and $[Nb_6O_{19}]^{8-}$, were reported to coordinate and form self-assembly monolayer on the surface of Au NPs, leading to the higher-energy shift of the LSPR band of Au NPs.[22, 23, 25-27] Thus, the LSPR energy shift in Fig. 3(A) indicated that the surface of supported Au NPs interacted with the $[Nb_6O_{19}]^{8-}$. X-ray photoelectron spectroscopy (XPS) suggested the electron donation from $[Nb_6O_{19}]^{8-}$ to Au NPs; the Au 4$f_{7/2}$ and 4$f_{5/2}$ signals of Au/Al_2O_3 assignable to the metallic Au^0 species were shifted to lower energy by the coordination of $[Nb_6O_{19}]^{8-}$ (Fig. 3B). Thus, we concluded that the $[Nb_6O_{19}]^{8-}$ modification on the surface of Au NPs results in the charge transfer from negatively charged oxygen atoms of metal oxide clusters to the Au NPs surface.

Next, the reduction of *p*-nitrophenol was carried out using various catalysts under the conditions described in Fig. 4 (H_2: 1 MPa, reaction temperature: 353 K, reaction time: 2 h). Among the catalysts

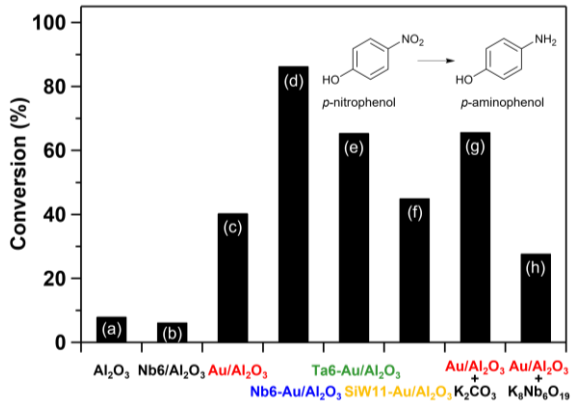

Fig. 4 Conversion of *p*-nitrophenol over (a) Al_2O_3, (b) Nb6/Al_2O_3, (c) Au/Al_2O_3, (d) Nb6-Au/Al_2O_3, (e) Ta6-Au/Al_2O_3, (f) SiW11-Au/Al_2O_3, and Au/Al_2O_3 with (g) K_2CO_3 and (h) $K_8Nb_6O_{19}$ addition as a base. Catalyst, 5 mg; substrate, 62.1 µmol; methanol, 1 mL; H_2, 1 MPa; reaction temperature, 353 K; reaction time, 2 h.

examined, Nb6-Au/Al_2O_3 exhibited the highest catalytic activity and afforded the desired *p*-aminophenol in 86% substrate conversion with >99% selectivity. The conversion reached >99% at 353 K for 18 h (Table S2). It should be noted that the catalytic activity of Nb6-Au/Al_2O_3 was much superior to that of unmodified Au/Al_2O_3. Nb6-Au/Al_2O_3 was reused several times though its catalytic performance gradually declined (Fig. S6). The reaction hardly proceeded when using Al_2O_3 or $[Nb_6O_{19}]^{8-}$-adsorbed Al_2O_3 (Nb6/Al_2O_3). In the Au/Al_2O_3-catalyzed reaction, the reaction rate increased when a base such as K_2CO_3 was added to the reaction solution, indicating that bases play an important role in the reduction of *p*-nitrophenol. $[Nb_6O_{19}]^{8-}$ is also known to function as a base catalyst; however, simply using Au/Al_2O_3 and $K_8Nb_6O_{19}$ as a physical mixture did not promote the reaction. Therefore, it is suggested that the catalyst design that lays out the basic $[Nb_6O_{19}]^{8-}$ species on or near Au NPs is crucially important for the reaction to proceed effectively.

In our catalyst design strategy reported herein, we believe that the catalytic activity can be fine-tuned by selecting the types of metal oxide clusters. We prepared several catalysts via the same method with different types of metal oxide clusters to investigate the generality of this approach. $[Ta_6O_{19}]^{8-}$-modified Au/Al_2O_3 (Ta6-Au/Al_2O_3) also showed higher activity than the pristine Au/Al_2O_3 because $[Ta_6O_{19}]^{8-}$ also has strong base catalysis.[19] However, Ta6-Au/Al_2O_3 was less active than Nb6-Au/Al_2O_3 although $[Ta_6O_{19}]^{8-}$ was higher basic strength than $[Nb_6O_{19}]^{8-}$. This is due to the prohibition of active sites on Au NPs by $[Ta_6O_{19}]^{8-}$ because $[Ta_6O_{19}]^{8-}$, which has more negatively charged oxygens than $[Nb_6O_{19}]^{8-}$,[19] adsorbed on Au NPs more than $[Nb_6O_{19}]^{8-}$ (Table S1). The modification of $[SiW_{11}O_{39}]^{8-}$, which also acts as a base catalyst but has weaker basicity and lower negatively-charged oxygens than $[Nb_6O_{19}]^{8-}$ and $[Ta_6O_{19}]^{8-}$,[30] with Au/Al_2O_3 (SiW11-Au/Al_2O_3) resulted in lower catalytic activity than Nb6-Au/Al_2O_3. From the XPS analysis, the Au $4f_{7/2}$ and $4f_{5/2}$ signals of Ta6-Au/Al_2O_3 and SiW11-Au/Al_2O_3 were located at lower energy than those of unmodified Au/Al_2O_3 (Fig. S7). Those lower-energy shifts indicated that $[Ta_6O_{19}]^{8-}$ and $[SiW_{11}O_{39}]^{8-}$ species were successfully modified on the surface of Au NPs. Therefore, the difference in the activities between the metal oxide clusters came from their base catalysis.

Table 1 Reaction results for reduction of nitro groups over metal-oxide-cluster-modified Au/Al_2O_3[a].

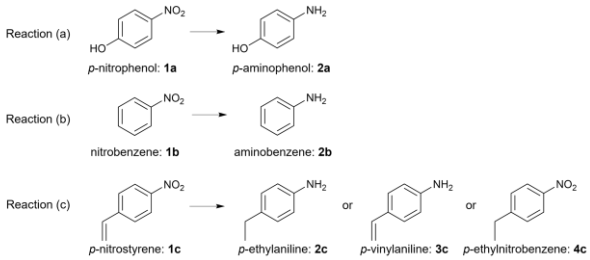

Entry	Reaction	Catalyst	Conversion (%)	Selectivity (%) (**2c**:**3c**:**4c**)
1	(a)	Nb6-Au/Al_2O_3	86	–
2		Au/Al_2O_3	40	–
3	(b)	Nb6-Au/Al_2O_3	43	–
4		Au/Al_2O_3	24	–
5	(c)	Nb6-Au/Al_2O_3	96	92:4:4
6		Au/Al_2O_3	21	3:97:<1

[a] Catalyst, 5 mg; substrate, 62.1 µmol; methanol, 1 mL; H_2, 1 MPa; reaction temperature, 353 K; reaction time, 2 h.

Several supported Au catalysts have known to be active in the reduction of aromatic nitro group compounds at 373–393 K using H_2 as a reductant.[1, 2, 31, 32] In the present case, Au/Al_2O_3 also showed catalytic activity for the reduction of *p*-nitrophenol in Fig. 4. In addition, we found that the addition of K_2CO_3 enhanced the reduction activity of Au/Al_2O_3. It was reported that the reduction of *p*-nitrophenol proceeds over Au NPs even at room temperature using $NaBH_4$ as a reductant.[32-35] $NaBH_4$ also acts as a base to promote the formation of nitrophenolate ion, followed by the reaction with cleaved hydrogen species formed on Au NPs to produce the desired *p*-aminophenol. K_2CO_3 would promote the formation of the nitrophenolate ion, resulting in accelerating the reduction. Previously, we reported that anionic Nb-based metal oxide clusters, such as $[Nb_6O_{19}]^{8-}$ and $[Ta_6O_{19}]^{8-}$, acted as efficient base catalysts for Knoevenagel condensation and CO_2 fixation reactions.[17-20] Thus, $[Nb_6O_{19}]^{8-}$ on Au/Al_2O_3 likely acts as a base catalyst to promote the formation of active nitrophenolate ions in the reaction. In addition, the interface between Au NPs and base $[Nb_6O_{19}]^{8-}$ contributes to the generation of active hydrogen species. Mitsudome *et al.* reported that the heterolytic cleavage of H_2 at the interface between metal and basic site produces polar hydrogen species, which selectively reduce the polar functional groups such as nitro groups.[7] Shimizu *et al.* reported that the reduction of *p*-nitrostyrene on Au/Al_2O_3 proceeded at the interface between Au NPs and Al_2O_3 by heterolytically cleaved hydrogen species and that the electron-enriched small Au NPs increased reactivity to H_2.[36] In the present catalyst, UV-Vis and XPS spectra revealed that negatively-charged Au NPs were formed by the electron donation from the coordinated $[Nb_6O_{19}]^{8-}$ to Au NPs in Nb6-Au/Al_2O_3 (Fig. 3A and B). Thus, the electron-rich Au surface or high density of $[Nb_6O_{19}]^{8-}$–Au NPs

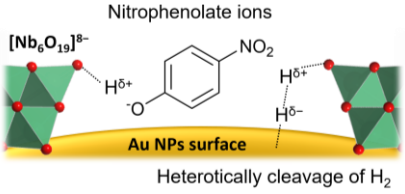

Fig. 5 Mechanism of *p*-nitrophenol reduction over Nb6-Au/Al_2O_3.

interface would effectively produce heterolytically cleaved hydrogen species that reacted with the nitrophenolate ions generated by the base catalysis (Fig. 5).

Finally, we applied Nb6-Au/Al_2O_3 catalyst to the reduction of several aromatic nitro compounds including *p*-nitrophenol (Table 1). The modification with $[Nb_6O_{19}]^{8-}$ improved the reduction conversions for not only *p*-nitrophenol but also nitrobenzene and *p*-nitrostyrene. In the reduction of *p*-nitrostyrene, Nb6-Au/Al_2O_3 selectively gave *p*-ethylaniline with byproducts of *p*-vinylaniline and *p*-ethylnitrobenzene after 2 h, whereas *p*-vinylaniline was mainly produced over Au/Al_2O_3. At lower conversion, Nb6-Au/Al_2O_3 showed high selectivity toward *p*-vinylaniline, and the *p*-ethylaniline selectivity increased with increasing the reaction time (Table S3, entries 1–3). In the case of Au/Al_2O_3, the *p*-ethylaniline selectivity also increased with time (Table S2, entries 1–3), consistent with the reported trend.[36] This suggests that the interface between Au NPs and basic $[Nb_6O_{19}]^{8-}$ efficiently produced the heterolytic cleaved hydrogen species, which promoted the reduction activities for both nitro and C=C groups.

Conflicts of interest

There are no conflicts to declare.

Acknowledgments

This research was financially supported by the Elements Strategy Initiative for Catalysts & Batteries (ESICB, JPMXP0112101003), Japan Society for the Promotion of Science (JSPS) KAKENHI (Nos. 18K18982, 20K22467, and 21H01718), JST PRESTO (Grant numbers JPMJPR18T7, and JPMJPR19T9), and Yazaki memorial foundation for science and technology. The XAFS measurements were conducted at SPring-8 with the approval of the Japan Synchrotron Radiation Research Institute (Nos. 2021A1272, 2021A1406, 2021B1373, and 2021B1535). We also thank Mr. Kang Xia (The University of Tokyo) for his assistance with the XPS and ICP-AES measurements.

Notes and references

1. A. Corma and P. Serna, *Science*, 2006, **313**, 332–334.
2. M. Boronat, P. Concepción, A. Corma, S. González, F. Illas and P. Serna, *J. Am. Chem. Soc.*, 2007, **129**, 16230–16237.
3. J. A. Delgado, O. Benkirane, C. Claver, D. Curulla-Ferre and C. Godard, *Dalton Trans*, 2017, **46**, 12381–12403.
4. F. Meemken and A. Baiker, *Chem. Rev.*, 2017, **117**, 11522–11569.
5. F. Zaera, *ACS Catal.*, 2017, **7**, 4947–4967.
6. L. Zhang, M. Zhou, A. Wang and T. Zhang, *Chem. Rev.*, 2020, **120**, 683–733.
7. T. Mitsudome, Y. Mikami, M. Matoba, T. Mizugaki, K. Jitsukawa and K. Kaneda, *Angew. Chem. Int. Ed.*, 2012, **51**, 136–139.
8. M. J. Sharif, P. Maity, S. Yamazoe and T. Tsukuda, *Chem. Lett.*, 2013, **42**, 1023–1025.
9. T. Yoskamtorn, S. Yamazoe, R. Takahata, J. Nishigaki, A. Thivasasith, J. Limtrakul and T. Tsukuda, *ACS Catal.*, 2014, **4**, 3696–3700.
10. G. A. Olah, J. Sommer and E. Namanworth, *J. Am. Chem. Soc.*, 1967, **89**, 3576–3581.
11. N. Mizuno and M. Misono, *Chem. Rev.*, 1998, **98**, 199–218.
12. K. Suzuki, N. Mizuno and K. Yamaguchi, *ACS Catal.*, 2018, **8**, 10809–10825.
13. Y. Iwase, O. Tomita, H. Naito, M. Higashi and R. Abe, *J. Photochem. Photobiol. A: Chem.*, 2018, **356**, 347–354.
14. K. Sugahara, T. Kimura, K. Kamata, K. Yamaguchi and N. Mizuno, *Chem. Commun.*, 2012, **48**, 8422–8424.
15. S. Itagaki, K. Kamata, K. Yamaguchi and N. Mizuno, *ChemCatChem*, 2013, **5**, 1725–1728.
16. A. Yoshida, S. Hikichi and N. Mizuno, *J. Organomet. Chem.*, 2007, **692**, 455–459.
17. S. Hayashi, S. Yamazoe, K. Koyasu and T. Tsukuda, *RSC Advances*, 2016, **6**, 16239–16242.
18. S. Hayashi, S. Yamazoe, K. Koyasu and T. Tsukuda, *Chem. Asian J*, 2017, **12**, 1635–1640.
19. S. Hayashi, N. Sasaki, S. Yamazoe and T. Tsukuda, *J. Phys. Chem. C*, 2018, **122**, 29398–29404.
20. S. Hayashi, S. Yamazoe and T. Tsukuda, *J. Phys. Chem. C*, 2020, **124**, 10975–10980.
21. Y. Tan, X. Y. Liu, L. Zhang, A. Wang, L. Li, X. Pan, S. Miao, M. Haruta, H. Wei, H. Wang, F. Wang, X. Wang and T. Zhang, *Angew. Chem. Int. Ed.*, 2017, **56**, 2709–2713.
22. A. Neyman, L. Meshi, L. Zeiri and I. A. Weinstock, *J. Am. Chem. Soc.*, 2008, **130**, 16480–16481.
23. Y. Wang, A. Neyman, E. Arkhangelsky, V. Gitis, L. Meshi and I. A. Weinstock, *J. Am. Chem. Soc.*, 2009, **131**, 17412–17422.
24. Y. Wang and I. A. Weinstock, *Dalton Trans*, 2010, **39**, 6143–6152.
25. Y. Wang, O. Zeiri, S. Sharet and I. A. Weinstock, *Inorg. Chem.*, 2012, **51**, 7436–7438.
26. M. Zhang, J. Hao, A. Neyman, Y. Wang and I. A. Weinstock, *Inorg. Chem.*, 2017, **56**, 2400–2408.
27. S. S. Leiser, L. Polin, G. GanOr, M. Raula and I. A. Weinstock, *Inorg. Chem.*, 2019, **58**, 1012–1015.
28. Y. Nakagawa, A. Kuwata, K. Yamaguchi, M. Tamura, M. Yabushita and K. Tomishige, *Inorg. Chem.*, 2021, **60**, 12413–12424.
29. S. Kikkawa, M. Tsukada, K. Shibata, Y. Fujiki, K. Shibusawa, J. Hirayama, N. Nakatani, T. Yamamoto and S. Yamazoe, *Symmetry*, 2021, **13**, 1267–1276.
30. M. Nyman, *Dalton Trans*, 2011, **40**, 8049–8058.
31. K. Wu, X. Wang, L. Guo, Y. Xu, L. Zhou, Z. Lyu, K. Liu, R. Si, Y. Zhang, L. Sun and C. Yan, *Nano Research*, 2020, **13**, 2044–2055.
32. B. Yu, B. Han, X. Jiang, C. Zhou, K. Xia, Q. Gao and J. Wu, *J. Phys. Chem. C*, 2019, **123**, 10389–10397.
33. D. Gao, X. Zhang, X. Dai, Y. Qin, A. Duan, Y. Yu, H. Zhuo, H. Zhao, P. Zhang, Y. Jiang, J. Li and Z. Zhao, *Nano Research*, 2016, **9**, 3099–3115.
34. P. Suchomel, L. Kvitek, R. Prucek, A. Panacek, A. Halder, S. Vajda and R. Zboril, *Sci. Rep.*, 2018, **8**, 4589–4599.
35. M. Zhang, Q. Liu, L. Sun, H. Su and C. Qi, *Catal. Lett.*, 2019, **150**, 438–449.
36. K. Shimizu, Y. Miyamoto, T. Kawasaki, T. Tanji, Y. Tai and A. Satsuma, *J. Phys. Chem. C*, 2009, **113**, 17803–17810.